Dynamics in liquids

2001 J. Phys.: Condens. Matter 13 7775

(http://iopscience.iop.org/0953-8984/13/34/320)

INSTITUTE OF PHYSICS PUBLISHING JOURNAL OF PHYSICS: CONDENSED MATTER

J. Phys.: Condens. Matter **13** (2001) 7775–7799 PII: S0953-8984(01)25893-7

Dynamics in liquids

Peter Verkerk[1]

Interfacultair Reactor Instituut, TUDelft, 2629 JB Delft, The Netherlands

Received 19 June 2001
Published 9 August 2001
Online at stacks.iop.org/JPhysCM/13/7775

Abstract

Some aspects of the theory of the dynamics in liquids are reviewed and compared with results from computer simulations and experiments. The range of liquids includes liquefied rare gases, binary mixtures, molten metals and molten alloys. A few of today's challenges regarding dynamics in liquids are listed.

1. Introduction

Our world is a fluid one and everything moves as Herakleitos ($\pi\alpha\nu\tau\alpha\ \rho\varepsilon\iota$) already noticed around 500 BC. I illustrate this with a few examples. The mere existence of life is based on fluids; chemical reactions are most efficient in the liquid state; the outer core as well as the mantle of the earth behave like fluids (although on very different time scales); the giant planets of the solar system are mainly fluid. Enough reasons to try to understand liquids and, for the fundamentals, in particular the dynamics on the atomic scale. The task of statistical physics is to predict macroscopic properties in terms of the microscopic properties of *individual* atoms or molecules. Until today the very nature of a liquid with its absence of long-range order as in a crystal or absence of ideal disorder as in a dilute gas prevented the development of a rigorous theory. Instead, theories for liquids are extrapolations of e.g. the exact theory for dilute gases to dense systems or of the well established macroscopic linearized hydrodynamic description down to the microscopic scale.

For more than 50 years inelastic neutron scattering has been the most suitable experimental tool to test theories of the microscopic structure and dynamics of condensed matter and of liquids in particular. This is due to the fact that the kinetic energy of 'thermalized' neutrons (25 meV at room temperature) and the mass are comparable to those of atoms and molecules in a liquid. This is not the case for photons: for x-rays the wavelength is of the order of intermolecular distances, but the photon energy is six orders of magnitude higher than the molecular thermal energies. For visible light the wavelength is three orders of magnitude larger than intermolecular distances and therefore light scattering is unable to probe molecular dynamics except in very dilute systems.

[1] Dr P Verkerk has unfortunately died as a result of a road accident.

With the advent of very intense photon sources in the form of third generation electron synchrotrons it is now possible to achieve an energy resolution $\Delta E/E = 10^{-7}$ (Burkel 1991). Therefore, ultra-high resolution inelastic x-ray scattering can now be used to investigate microscopic dynamics with an energy resolution of 1 meV, which opens entirely new possibilities. Because of the different properties of neutrons and x-rays, inelastic neutron scattering and inelastic x-ray scattering form a useful complementary pair.

Our understanding of the dynamics in liquids has also benefited considerably from molecular dynamics (MD) computer simulations. By solving Newton's equations of motion for a limited number of particles interacting through a model potential one calculates on one hand the same quantities that are measured experimentally and in addition any other microscopic quantity which is inaccessible for experiment. MD simulations are useful for verifying theories because they both can use identical models for the interaction potentials. MD simulations also serve to interpret experimental data.

Section 2 gives examples of theories for liquid dynamics. Section 3 gives results from recent inelastic scattering experiments with neutrons as well as x-rays, and from MD simulations.

2. Theory

2.1. Definitions

A useful quantity describing molecular dynamics in condensed matter is Van Hove's time–dependent density–density correlation function:

$$G(\vec{r},t) = \frac{1}{\rho}\langle\rho(\vec{0},0)\rho(\vec{r},t)\rangle \tag{1}$$

with $\langle\cdots\rangle$ the ensemble average. The instantaneous local particle number density is given by

$$\rho(\vec{r},t) = \sum_{j=1}^{N}\delta\{\vec{r}-\vec{R}_j(t)\}$$

with $\vec{R}_j(t)$ the position of the jth particle at time t, and the average density is $\rho = \langle\rho(\vec{r},t)\rangle$. The so-called self-part of $G(\vec{r},t)$ is defined by

$$G_s(\vec{r},t) = \langle\rho^1(\vec{0},0)\rho^1(\vec{r},t)\rangle \tag{2}$$

with the one-particle density

$$\rho^1(\vec{r},t) = \delta\{\vec{r}-\vec{R}'(t)\}$$

where $\vec{R}'(t)$ is the position of a marked particle. Associated with the microscopic number density we have the particle current:

$$\vec{j}(\vec{r},t) = \sum_{l=1}^{N}\vec{v}_l(t)\delta\{\vec{r}-\vec{r}_l(t)\} \qquad \vec{j}^1(\vec{r},t) = \vec{v}'(t)\delta\{\vec{r}-\vec{R}'(t)\}$$

where $\vec{v}_l(t)$ is the velocity of particle l, and $\vec{v}'(t)$ the velocity of a marked particle. The velocity autocorrelation function is defined as

$$Z(t) = \tfrac{1}{3}\langle\vec{v}'(t)\vec{v}'(0)\rangle. \tag{3}$$

The spatial Fourier transforms of equations (1) and (2) are called the intermediate scattering functions:

$$F(\vec{k},t) = \frac{1}{N}\langle\rho^*_{\vec{k}}\rho_{\vec{k}}(t)\rangle \qquad F_s(\vec{k},t) = \langle\rho^{1*}_{\vec{k}}\rho^1_{\vec{k}}(t)\rangle \tag{4}$$

where $\rho_{\vec{k}}(t)$ and $\rho^1_{\vec{k}}(t)$ are plane waves of density fluctuations with wavevector $\vec{k}$:

$$\rho_{\vec{k}}(t) = \sum_{j=1}^{N} \exp[\mathrm{i}\vec{k}\vec{R}_j(t)] \qquad \rho^1_{\vec{k}}(t) = \exp[\mathrm{i}\vec{k}\vec{R}'(t)].$$

The associated Fourier components of the particle currents are

$$\vec{j}_{\vec{k}}(t) = \sum_{l=1}^{N} \vec{v}_l(t) \exp[\mathrm{i}\vec{k}\vec{R}_l(t)] \qquad \vec{j}^1_{\vec{k}}(t) = \vec{v}'(t) \exp[\mathrm{i}\vec{k}\vec{R}'(t)]$$

which can be split in a transverse component $j^T_{\vec{k}}(t)$ perpendicular to $\vec{k}$ and a longitudinal component $j^z_{\vec{k}}(t)$ parallel to $\vec{k}$, assuming the system is isotropic. Analogous to the density correlation functions we define the transverse and the longitudinal current–current correlation functions:

$$C_T(\vec{k}, t) = \frac{1}{2N}\langle j^{T^*}_{\vec{k}}(0) j^T_{\vec{k}}(t)\rangle = \frac{1}{N}\langle j^{x^*}_{\vec{k}}(0) j^x_{\vec{k}}(t)\rangle = \frac{1}{N}\langle j^{y^*}_{\vec{k}}(0) j^y_{\vec{k}}(t)\rangle \tag{5}$$

$$C_L(\vec{k}, t) = \frac{1}{N}\langle j^{z^*}_{\vec{k}}(0) j^z_{\vec{k}}(t)\rangle. \tag{6}$$

Fourier transforming equations (4) from t to ω leads to the dynamical structure factors:

$$S_{(s)}(\vec{k}, \omega) = \frac{1}{2\pi}\int_{-\infty}^{\infty} F_{(s)}(\vec{k}, t) \exp(\mathrm{i}\omega t)\, \mathrm{d}t. \tag{7}$$

$S(k, \omega)$ can be measured by inelastic neutron as well as x-ray scattering, but $S_s(k, \omega)$ can only be measured by neutrons. For both types of scattering experiment $\hbar k$ is the momentum transfer and $\hbar\omega$ the energy transfer. In isotropic media as liquids and gases the scattering functions depend only on $k = |\vec{k}|$. From the definitions it follows that $\dot{\rho}_{\vec{k}}(t) = \mathrm{i}k j^z_{\vec{k}}(t)$ and the longitudinal current correlation function is related to the density correlation function:

$$C_L(\vec{k}, t) = -\frac{1}{k^2}\ddot{F}(k, t). \tag{8}$$

The Fourier transform of equation (8) is

$$\tilde{C}_L(k, \omega) = \frac{\omega^2}{k^2} S(k, \omega). \tag{9}$$

Expanding the intermediate scattering functions in a Taylor series at $t = 0$, we get for the coefficients

$$\left[\frac{\mathrm{d}^n F_{(s)}(k, t)}{\mathrm{d}t^n}\right]_{t=0} = (-\mathrm{i})^n \int_{-\infty}^{\infty} \omega^n S_{(s)}(k, \omega)\, \mathrm{d}\omega = (-\mathrm{i})^n \langle\omega^n\rangle_{(s)}. \tag{10}$$

The lowest order frequency moments $\langle\omega^n\rangle$ and $\langle\omega^n\rangle_s$ have been calculated:

$$\begin{aligned}
&\langle\omega^0\rangle = S(k) \qquad \langle\omega^0\rangle_s = 1 \\
&\langle\omega\rangle = \langle\omega\rangle_s = \omega_R = \frac{\hbar k^2}{2M} \\
&\langle\omega^2\rangle = \langle\omega^2\rangle_s = \frac{k_B T}{M} k^2 + \mathrm{O}(\hbar^2)
\end{aligned} \tag{11}$$

with M the particle mass, T the temperature, k_B Boltzmann's constant and $\hbar\omega_R$ the recoil energy, the average energy imparted by the scattered photon or neutron to the system. The third and fourth frequency moments have been calculated for an additive two-particle interaction potential $\varphi(r)$ (Puff 1965, DeGennes 1959):

$$\begin{aligned}
&\langle\omega^3\rangle = \omega_R\{\omega_R[\omega_R + 4\omega_K] + \Omega^2(k)\} \\
&\langle\omega^4\rangle = \langle\omega^2\rangle\{3\langle\omega^2\rangle + \Omega^2(k)\} + \mathrm{O}(\hbar^2)
\end{aligned} \tag{12}$$

with $\hbar\omega_K$ the average kinetic energy per particle and

$$\Omega^2(k) = \frac{\rho}{M}\int\{1-\cos(kz)\}\frac{\mathrm{d}^2\varphi(r)}{\mathrm{d}z^2}g(r)\,\mathrm{d}\vec{r} \tag{13}$$

with $g(r)$ the static pair distribution function.

A rigorous property of $S(k,\omega)$ is the condition of detailed balance:

$$S(k,-\omega) = \exp\left(-\frac{\hbar\omega}{k_BT}\right)S(k,\omega). \tag{14}$$

In classical theories $S(k,\omega)$ is an even function of ω, i.e. $G(r,t)$ and $F(k,t)$ are real functions, and one possibility to relate classical theory to real systems is to approach a symmetrized version of $S(k,\omega)$ by the classical one. For instance

$$S_{class.}(k,\omega) = S_{sym}(k,\omega) = \frac{1-\exp(-\hbar\omega/k_BT)}{\hbar\omega/k_BT}S(k,\omega). \tag{15}$$

2.2. Solid-like behaviour

2.2.1. Visco-elastic model. As an illustration of how theories for liquids may be developed we begin with the visco-elastic model, which is relatively simple but has been very successful in the description of the dynamics in liquids. Frenkel (1946) considered the connection between viscosity and the rigidity of liquid bodies using Maxwell's relaxation theory of elasticity (Maxwell 1867). If a shearing force is applied to a liquid, the stress tensor is proportional to the velocity gradient:

$$\sigma^{\alpha\beta} = -\eta\left(\frac{\partial v_\alpha}{\partial r_\beta}+\frac{\partial v_\beta}{\partial r_\alpha}\right) \tag{16}$$

with η the shear viscosity, and $\alpha,\beta = x, y$ or z. However, if the force is applied suddenly, the liquid behaves like a solid, and the stress is proportional to the strain, i.e. the displacement of adjacent layers with respect to each other:

$$\sigma^{\alpha\beta} = -G\left(\frac{\partial u_\alpha}{\partial r_\beta}+\frac{\partial u_\beta}{\partial r_\alpha}\right) \tag{17}$$

where u_α is the displacement with respect to equilibrium and G the rigidity modulus. Interpolating between equations (16) and (17) it is possible to write

$$-\left(\frac{\partial v_\alpha}{\partial r_\beta}+\frac{\partial v_\beta}{\partial r_\alpha}\right) = \frac{1}{G}\frac{\mathrm{d}\sigma^{\alpha\beta}}{\mathrm{d}t}+\frac{1}{\eta}\sigma^{\alpha\beta}. \tag{18}$$

If at $t=0$ the motion suddenly stops, i.e. $\vec{v}=0$, the solution for equation (18) is

$$\sigma^{\alpha\beta}(t) = \sigma^{\alpha\beta}(0)\exp(-t/\tau_M)$$

so the stress relaxes with Maxwell's relaxation time $\tau_M = \eta/G$. Substituting

$$\eta(t) = G\exp(-t/\tau_M) \tag{19}$$

in equation (16) is equivalent to Maxwell's visco-elastic approximation. If the shear force changes rapidly, and the stress has no time to relax, elastic waves will be generated, while at low frequency the liquid will perform viscous flow. Obviously, visco-elastic effects can occur only in the transverse component of the current $\vec{j}_{\vec{k}}(t)$, and therefore the visco-elastic approximation has consequences for the transverse current correlation function $C_T(k,t)$. From the Navier–Stokes equations, which describe the dynamics in a liquid on a macroscopic scale ($k\to 0$) it follows that

$$\frac{\partial}{\partial t}C_T(k,t)+\nu k^2 C_T(k,t) = 0 \tag{20}$$

with $\nu = \eta/(\rho M)$ the kinematic shear viscosity, and the solution to this equation is

$$C_T(k,t) = C_T(k,0)\exp(-\nu k^2 t).$$

This result has been generalized (e.g. Ailawadi *et al* 1971) by introducing a generalized viscosity or memory function:

$$\frac{\partial}{\partial t}C_T(k,t) + k^2 \int_0^t \mathrm{d}s\, \nu(k,t-s)C_T(k,s) = 0 \tag{21}$$

and using a k-dependent relaxation time $\tau_M(k)$, i.e. assuming a functional form for the generalized viscosity as

$$\nu(k,t) = \frac{G}{\rho M}\exp[-t/\tau_M(k)].$$

Laplace transforming equation (21), the solution for the transverse current correlation function is easily obtained as

$$\hat{C}_T(k,z) = \frac{C_T(k,t=0)}{-\mathrm{i}z + k^2\hat{\nu}(k,z)} = \frac{\langle\omega^2\rangle}{-\mathrm{i}z + k^2\hat{\nu}(k,z)} \tag{22}$$

with

$$\hat{\nu}(k,z) = \frac{G/(\rho M)}{z + 1/\tau_M(k)}.$$

Since the transverse current correlation function is not accessible to experimental techniques, only computer simulations can test the visco-elastic model. This has been done by Levesque *et al* (1973) for a fluid of particles interacting through the Lennard-Jones potential. Given the simplicity of the visco-elastic model the agreement was very satisfactory. In particular, the occurrence in the computer simulations of shear waves showing as peaks in $\tilde{C}_T(k,\omega)$ is predicted by the visco-elastic model.

In view of this success, a similar approximation was proposed (Ailawadi *et al* 1971) for the longitudinal currents, starting again from the Navier–Stokes equations:

$$\frac{\partial}{\partial t}C_L(k,t) + \int_0^t \mathrm{d}s\, K(k,t-s)C_L(k,s) = 0 \tag{23}$$

with

$$K(k,t) = k^2\left[\frac{k_B T}{MS(k)} + \psi(k,t)\right] \tag{24}$$

and

$$\hat{\psi}(k,z) = \frac{\psi(k,t=0)}{z + 1/\tau(k)} \tag{25}$$

where the initial value of $\psi(k,t)$ can again be obtained from the thermodynamic and structural properties of the liquid, and $\tau(k)$ is a 'longitudinal' relaxation time.

This expression leads, through equation (9), to a model for the dynamic structure factor that has been widely used in the literature.

2.2.2. Damped harmonic oscillator. This is another model used for liquids and related to the solid state. It is obtained studying a single nucleus bound in a damped harmonic oscillator (Crevecoeur *et al* 1996) and considering only the first excited state. The dynamic structure factor is

$$S(k,\omega) = \frac{A}{2\pi\Gamma}\frac{\hbar\omega/k_B T}{1-\exp(-k_B T/\hbar\omega)}\frac{4\Omega^2\Gamma^2}{(\omega^2-\Omega^2)^2 + (2\omega\Gamma)^2}. \tag{26}$$

Using equation (15) the symmetrized $S(k, \omega)$ can be written as

$$S_{sym}(k, \omega) = \frac{A}{2\pi} \left\{ \frac{\Gamma + (\omega + \omega_s) \tan \varphi}{(\omega + \omega_s)^2 + \Gamma^2} + \frac{\Gamma - (\omega - \omega_s) \tan \varphi}{(\omega - \omega_s)^2 + \Gamma^2} \right\} \tag{27}$$

with $\omega_s^2 = \Omega^2 - \Gamma^2$, $\tan \varphi = \Gamma/\omega_s$. The Fourier transform is

$$F(k, t) = \frac{1}{\cos \varphi} \exp(-\Gamma|t|) \cos(\omega_s|t| - \varphi) \tag{28}$$

which oscillates as function of t with frequency ω_s, damping coefficient Γ and phase shift φ. This result maybe generalized by making ω_s and Γ k dependent, and it has been used to analyse e.g. data for liquid He (Crevecoeur *et al* 1996) or phonon-like excitations in classical liquids like argon (de Schepper *et al* 1983).

2.3. From hydrodynamics to microscopic dynamics

On a macroscopic scale there are five independent conserved variables, for instance the number density ρ, momentum density $\vec{p} = m\vec{v}$ and energy density e. This choice is rather obvious, but other choices, for instance ρ, the longitudinal velocity v parallel to $\vec{k}$, local temperature, fluctuations of the longitudinal stress tensor and fluctuations of the longitudinal heat current, are also possible and their use is sometimes advantageous. For a binary mixture a possible choice is the relative concentration of one component, the total number density, total momentum density, temperature, and relative velocity.

In the case of $S_s(k, \omega)$ we are only concerned with the one-particle density $\rho^1(\vec{r}, t)$. Combination of the conservation law and the constitutive relation, which defines the self-diffusion coefficient D, leads to

$$S_s(k, \omega) = \frac{1}{\pi} \frac{Dk^2}{\omega^2 + (Dk^2)^2} \qquad F_s(k, t) = \exp(-Dk^2|t|). \tag{29}$$

This is valid for the macroscopic case, i.e. $k \to 0$. From section 2.1 it follows that

$$Z(t) = -\lim_{k \to 0} \frac{1}{k^2} \frac{\mathrm{d}^2}{\mathrm{d}t^2} F_s(k, t) \qquad \tilde{Z}(\omega) = \omega^2 \lim_{k \to 0} \frac{S_s(k, \omega)}{k^2}. \tag{30}$$

In other words, a measurement of $S_s(k, \omega)$ in the hydrodynamic regime yields $\tilde{Z}(\omega)$. In order to avoid divergence at $\omega = 0$ in determining $\tilde{Z}(\omega)$ from experimental data it is better to replace the second equation in (30) by

$$\tilde{Z}(\omega) = \frac{D}{\pi} \lim_{k \to 0} Z(k, \omega) \qquad Z(k, \omega) = \left[\frac{1}{\pi} \frac{Dk^2}{\omega^2 + (Dk^2)^2} \right]^{-1} S_s(k, \omega). \tag{31}$$

The limit $k \to 0$ in the previous equations is not a trivial task from the experimental point of view, and different limiting procedures can lead sometimes to somewhat different results. The two most common limiting methods are linear extrapolation and quadratic extrapolation, the latter being supported by mode-coupling theories (see below).

For $S(k, \omega)$ in the hydrodynamic regime, we use number density, momentum density and temperature as the conserved variables. Using the Navier–Stokes equations, which introduce the transport coefficients shear viscosity, bulk viscosity and thermal conductivity, and neglecting all but the first order in the deviations of local density, momentum and energy (or temperature) from their average values, we get after taking the Fourier–Laplace transform to (k, z)

$$\mathbf{H}(k, z) \cdot \tilde{\vec{A}}_{\vec{k}}(z) = \vec{A}_{\vec{k}}(t = 0) \tag{32}$$

where $\vec{A}_{\vec{k}}(t) = \{\rho_{\vec{k}}(t), T_{\vec{k}}(t), \vec{j}_{\vec{k}}(t)\}$. The 5×5 hydrodynamic matrix $\mathbf{H}(k, z)$ is given by

$$\begin{pmatrix} -\mathrm{i}z & 0 & \mathrm{i}k & 0 & 0 \\ 0 & -\mathrm{i}z + ak^2 & \mathrm{i}f_{j^z,T}(k) & 0 & 0 \\ \mathrm{i}f_{\rho,j^z}(k) & \mathrm{i}f_{T,j^z}(k) & -\mathrm{i}z + bk^2 & 0 & 0 \\ 0 & 0 & 0 & -\mathrm{i}z + \nu k^2 & 0 \\ 0 & 0 & 0 & 0 & -\mathrm{i}z + \nu k^2 \end{pmatrix} \tag{33}$$

with the kinematic shear viscosity $\nu = \eta/(\rho M)$, the coefficient $b = (4\eta/3 + \zeta)/(\rho M)$, where ζ is the bulk viscosity, the coefficient $a = \lambda/(\rho c_V)$, where λ is the thermal conductivity and $\gamma = c_P/c_V$. The real functions $f_{i,j}(k)$ are determined by thermodynamics and from the elements of $\mathbf{\Omega}$ in equation (43). The transverse currents j^x and j^y are completely decoupled from the other three variables. Therefore, equation (32) splits in a set of three equations for $\{\tilde{\rho}_{\vec{k}}(z), \tilde{T}_{\vec{k}}(z), \tilde{j}^z_{\vec{k}}(z)\}$ and a set of two equations for $\{\tilde{j}^x_{\vec{k}}(z), \tilde{j}^y_{\vec{k}}(z)\}$. The density ρ and the longitudinal current j^z are coupled, the same for the temperature T and j^z, but ρ and T are not coupled. Solving for $\tilde{\rho}_{\vec{k}}(z)$ and using

$$S(k, \omega) = \frac{1}{\pi}\mathrm{Re}\,\langle \rho_{\vec{k}}(t = 0)\tilde{\rho}_{\vec{k}}(z = \mathrm{i}\omega)\rangle$$

leads to the well known Rayleigh–Brillouin triplet:

$$2\pi\frac{S(k,\omega)}{S(k)} = \left(\frac{\gamma - 1}{\gamma}\right)\frac{2D_T k^2}{\omega^2 + (D_T k^2)^2} + \frac{1}{\gamma}\left\{\frac{\Gamma k^2 + (\omega + c_s k)b_s k}{(\omega + c_s k)^2 + (\Gamma k^2)^2} + \frac{\Gamma k^2 - (\omega - c_s k)b_s k}{(\omega - c_s k)^2 + (\Gamma k^2)^2}\right\} \tag{34}$$

with $\Gamma = [a(\gamma - 1)/\gamma + b]/2$ the sound attenuation coefficient, c_s the adiabatic sound velocity, $b_s = [(\gamma - 1)a + \Gamma]/c_s$ and $D_T = a/\gamma$ the thermal diffusivity. The second term of the right hand side is identical to the result for the damped harmonic oscillator. Note that in general equation (34) has a divergent second frequency moment $\langle\omega^2\rangle$ and therefore does not lead to the correct short-time behaviour.

Solving equation (32) for $\tilde{j}^x_{\vec{k}}(z)$ we obtain for the transverse current correlation function $\tilde{C}_T(k, \omega) = \mathrm{Re}\,[\hat{C}_T(k, z = \mathrm{i}\omega)]$:

$$\hat{C}_T(k, z) = \langle\omega^2\rangle\left[-\mathrm{i}z + bk^2 + c_s^2 k^2\left(\frac{1}{-\mathrm{i}z} + \frac{\gamma - 1}{-\mathrm{i}z + ak^2}\right)\right]^{-1}. \tag{35}$$

In order to extend the hydrodynamic results to larger k and short t, frequency and wavenumber dependent transport coefficients have been introduced leading to *generalized hydrodynamics*. Examples have already been given in section 2.2.1 for the current correlation functions.

2.4. From dilute gas to liquid

For a gas of non-interacting particles obeying Boltzmann statistics we have

$$S(k, \omega) = S_s(k, \omega) = \frac{1}{k}\sqrt{\frac{M}{2\pi k_B T}}\exp\left\{-\frac{M}{2k_B T k^2}\left(\omega - \frac{\hbar k^2}{2M}\right)^2\right\}. \tag{36}$$

Equation (36) is also valid for any density in the limit $k \to \infty$, where the wavelength $\lambda = 2\pi/k$ of the observed Fourier components $\rho_{\vec{k}}(t)$ of the density fluctuations is so small that only the behaviour of the particles on a very short length scale counts and the interactions between the particles are irrelevant.

A first step towards real liquids is the inclusion of uncorrelated binary collisions and we arrive at Boltzmann's kinetic equation. His approximation is valid for a dilute gas.

The scattering functions are obtained in terms of collision integrals, which can be evaluated numerically for arbitrary two-particle interaction potentials (Maitland *et al* 1981).

The Boltzmann equation for hard spheres was modified semi-empirically by Enskog (Chapman and Cowling 1970), and was revised by van Beijeren and Ernst (1973, 1979). The same assumptions as in the Boltzmann theory apply (collisions between particles are binary and successive collisions are uncorrelated), but corrections for the static structure of the liquid and the finite size of the particles are applied.

As in the case of hydrodynamics we choose the set of variables that are conserved in the hydrodynamic (macroscopic) limit and which determine $S(k,\omega)$ (see e.g. Cohen and de Schepper 1990): number density, longitudinal current and temperature, adequately renormalized. Now we use $\tilde{A}_{\vec{k}}(t) = \{\rho^R_{\vec{k}}(t), j^{z^R}_{\vec{k}}(t), T^R_{\vec{k}}(t)\}$. The nine correlation functions are given by

$$F^R_{\alpha\beta}(k,t) = \langle A^*_{\vec{k},\alpha}(t=0) A_{\vec{k},\beta}(t)\rangle = \langle A^*_{\vec{k},\alpha}\, \mathrm{e}^{L_N t}\, A_{\vec{k},\beta}\rangle \tag{37}$$

where the dynamic variable without argument denotes its value at $t = 0$. The renormalization (superscript R) is such that the initial value of the correlation functions is unity. We have also introduced an N-particle pseudo-Liouville operator, L_N, which describes the time evolution of any dynamic variable, $A_{\vec{k},\beta}(t) = \mathrm{e}^{L_N t}\, A_{\vec{k},\beta}$. Note that $F(k,t) = S(k) F^R_{\rho\rho}(k,t)$.

An approximate solution is found replacing the N-particle pseudo-Liouville operator by the Enskog operator $L_E(\vec{k})$, which takes only binary collisions into account and is a single-particle operator. Therefore, equation (37) can be simplified to

$$F^R_{\alpha\beta}(k,t) \approx \langle A'^*_{\vec{k},\alpha}\, \mathrm{e}^{tL_E(\vec{k})}\, A'_{\vec{k},\beta}\rangle_1 \tag{38}$$

where $\vec{A}'_{\vec{k}}$ is the one-particle analogue to $\vec{A}_{\vec{k}}$

$$\vec{A}'_{\vec{k}} = \left\{1, \sqrt{\frac{M}{k_B T}}\frac{\vec{k}\vec{v}}{k}, \sqrt{\frac{3}{2}}\left(\frac{3}{2} - \frac{Mv^2}{2k_B T}\right)\right\}$$

and $\langle\cdots\rangle_1$ denotes the average over the particle velocity, obtained through the Maxwell velocity distribution function:

$$\langle\cdots\rangle_1 = \int \mathrm{d}\vec{v}\cdots\left(\frac{M}{2\pi k_B T}\right)^{3/2} \exp\left[-\frac{Mv^2}{2k_B T}\right].$$

The inhomogeneous Enskog collision operator consists of three parts

$$L_E(\vec{k}) = -\mathrm{i}\vec{k}\vec{v} + \rho g(d)\Lambda_{\vec{k}} + \rho A_{\vec{k}}. \tag{39}$$

Here $-\mathrm{i}\vec{k}\vec{v}$ represents the free streaming part (free gas), $\Lambda_{\vec{k}}$ is the binary collision operator, $g(d)$ the hard-sphere pair correlation function at contact and $A_{\vec{k}}$ the mean field part, that incorporates through $S(k)$ the effect of a mean field in which each hard sphere moves due to the presence of the other hard spheres. $F_{\alpha\beta}(k,t)$ is evaluated by determining the eigenvalues $z_j(k)$ of $L_E(k)$.

In the particular case of the dynamic structure factor the result is

$$S(k,\omega) = \frac{S(k)}{\pi}\,\mathrm{Re}\,\langle[\mathrm{i}\omega - L_E(k)]^{-1}\rangle_1 = \frac{S(k)}{\pi}\,\mathrm{Re}\sum_j \frac{M_j(k)}{\mathrm{i}\omega - z_j(k)}. \tag{40}$$

In the $k \to 0$ limit three of the terms, usually denoted by $j = 0, \pm 1$, reproduce the hydrodynamic expression with the transport coefficients replaced by their Enskog counterparts, whereas the amplitude $M_j(k)$ of all the other terms go to zero in this limit.

Up to 12 eigenvalues have been calculated. However, it turns out that outside the hydrodynamic regime, but still $kl_E < 1$, $S(k,\omega)$ can be represented by three effective extended hydrodynamic modes, which reduce to the three hydrodynamic modes for small k. We have

introduced here the Enskog mean free path, $l_E = l_0/g(d)$, where $l_0 = 1/(\rho\pi d^2\sqrt{2})$ is the standard mean free path for hard spheres of diameter d.

For low density $L_E(\vec{k})$ approaches the Boltzmann collision operator $L_B(\vec{k}) = -\mathrm{i}\vec{k}\vec{v}+\rho\Lambda_{\vec{k}}$. For large k, i.e. $kl_{mf} \gg 1$, where $l_{mf} = l_0$ for low density, or $l_{mf} = l_E$ for arbitrary density, the operator $[\mathrm{i}\omega - L_\alpha(\vec{k})]^{-1}$ with $\alpha = E$ or B, can be expanded around the free streaming term leading to a series of binary collisions (Kamgar-Parsi *et al* 1987):

$$S(k,\omega) = \frac{2}{\pi}\frac{t_{mf}}{kl_{mf}}\left[\exp\left(-\frac{4}{\pi}(\omega^*)^2\right) + \frac{s_{11}^\alpha(\omega^*)}{kl_{mf}} + \mathrm{O}\left(\left(\frac{1}{kl_{mf}}\right)^2\right)\right] \tag{41}$$

with $\omega^* = \omega t_{mf}/(kl_{mf})$ where again $t_{mf} = t_0$ for low density, or $t_{mf} = t_E = t_0/g(d)$ for arbitrary density, with the mean free time between collisions

$$t_0 = \frac{1}{4\rho d^2}\sqrt{\frac{M}{\pi k_B T}}.$$

Equation (41) is a first-order correction to the free gas model (first term) and can be regarded either as an expansion in $1/k$ or in the density. The function $s_{11}^\alpha(\omega^*)$ does not explicitly depend on T, ρ or k, only on ω^*. The result for $S_s(k,\omega)$ can be obtained from equation (41) replacing $s_{11}^\alpha(\omega^*)$ by the corresponding function $s^\alpha(\omega^*)$. These two functions for the low-density case ($\alpha = B$) have been calculated numerically.

Because the Enskog collision operator takes into account only binary collisions, the so-called ring collisions are neglected. In such an event a tagged particle collides with another particle, then propagates through the fluid, colliding with various other particles, and then recollides with the same particle it met initially. Such effects are particularly important in self-diffusion.

2.4.1. Binary mixtures. Westerhuijs *et al* (1992) derived an expression for a binary mixture of hard spheres using an approach similar to the Enskog theory for a one-component system. They use five basic variables: number concentration, total number density, total momentum, temperature and mutual relative velocity of the constituents. The result is as in equation (40) but the sum involves only five terms. For k outside the hydrodynamic regime one of the roots z_j is real and corresponds to an elastic line, whereas the other four roots are two pairs of complex conjugate roots, corresponding to two pairs of inelastic lines. The central one corresponds to correlations in the concentration fluctuations, while the inelastic lines represent two types of propagating mode. There are therefore two slow and two fast modes at frequencies $\pm\omega_s(k)$ and $\pm\omega_f(k)$. In the hydrodynamic region the frequency of the fast mode becomes zero, so that the roots turn real, and thus the structure of the solution is three real roots and a pair of complex conjugate roots. Four of them reduce to the hydrodynamic modes, with the transport coefficients replaced by their Enskog analogues, whereas the other one, which corresponds to the mutual velocity, disappears because it is not a conserved quantity; this means that the corresponding amplitude in equation (40) goes to zero. Then we have a sum of four Lorentzians, two elastic ones with a width determined by respectively the concentration diffusion coefficient and the thermal diffusivity, and two inelastic lines at frequencies determined by the 'hydrodynamic' sound velocity $\pm c_s k$, with a width determined by the sound attenuation.

2.5. Memory functions

The time evolution of a variable $A(\vec{r}^N(t), \vec{p}^N(t))$ is formally given by the Liouville equation:

$$A(t) = \exp(\mathrm{i}\mathcal{L}t)A(0)$$

or

$$\frac{\mathrm{d}A(t)}{\mathrm{d}t} = \exp(\mathrm{i}\mathcal{L}t)\mathrm{i}\mathcal{L}A(0) \tag{42}$$

where Λ is the ordinary Liouville operator, N the number of particles and $(\vec{r}_j, \vec{p}_j)$ the coordinates of particle j in phase space. Of course it is impossible to solve the Liouville equation exactly in terms of $6N$ variables. A very useful and generally applied approach is to choose a set of variables $A(t)$ slowly varying with time. Then an operator Π is defined which projects any variable $B(t)$ on the subspace spanned by $A(t=0)$:

$$\mathcal{P}B(t) = \langle A^* B(t)\rangle \langle A^* A\rangle^{-1} A.$$

Then the right hand side of equation (42) is modified by inserting the identity operator $\Pi + (1 - \Pi)$ after the operator $\exp(\mathrm{i}\mathcal{L}t)$. It is believed that a good choice of A is the set of variables that are conserved in hydrodynamics: number of particles, momentum and energy. On the microscopic scale these variables are not at all conserved, but they will be slowly varying or quasi-conserved at least for small k.

For the correlation function $\boldsymbol{C}(t) = \langle \vec{A}^*(0)\vec{A}(t)\rangle$ the procedure described above leads to the memory function approach (Hansen and McDonald 1986):

$$\frac{\mathrm{d}\boldsymbol{C}(t)}{\mathrm{d}t} = \mathrm{i}\boldsymbol{\Omega}\cdot\boldsymbol{C}(t) - \int_0^t \mathrm{d}s\, \boldsymbol{M}(t-s)\cdot\boldsymbol{C}(s) \tag{43}$$

where $\boldsymbol{\Omega}$ has the dimension of a frequency and its elements depend only on equilibrium statistical averages. The second term on the right hand side of equation (43) is due to $1 - \Pi$. In fact the memory function $\boldsymbol{M}(t)$ is the autocorrelation function of a generalized random force $\vec{K}$ which is orthogonal to the set of slowly varying variables. Therefore, we expect that $\boldsymbol{M}(t)$ is decaying considerably faster than $\boldsymbol{C}(t)$, which may allow for simple approximations leading to useful results for the dynamics of the quasi-conserved variables.

Equation (43) can be solved by the Laplace transform and the solution reads

$$\hat{\boldsymbol{C}}(z) = \boldsymbol{C}(t=0)\cdot[z\boldsymbol{I} - \mathrm{i}\boldsymbol{\Omega} + \hat{\boldsymbol{M}}(z)]^{-1}. \tag{44}$$

2.5.1. Single-particle motion. As an illustration of the projection operator formalism, we return to the case of single-particle motion and self-diffusion. From the definitions of $\rho^1_{\vec{k}}(t)$ and $j^1_{\vec{k}}(t)$ in section 2.1 it follows that

$$\dot{\rho}^1_{\vec{k}}(t) = -\mathrm{i}\vec{k}\vec{j}^1_{\vec{k}}(t). \tag{45}$$

We choose to project on the single-particle density at $t = 0$, meaning that

$$\mathcal{P}B(t) = \langle \rho^{1^*}_{\vec{k}} B(t)\rangle \langle \rho^{1^*}_{\vec{k}} \rho^1_{\vec{k}}\rangle^{-1} \rho^1_{\vec{k}}. \tag{46}$$

In this particular case $\boldsymbol{\Omega}$ vanishes and

$$\dot{F}_s(k,t) = -\int_0^t \mathrm{d}s\, M_s(k, t-s)F_s(k,s). \tag{47}$$

It turns out that $M_s(k,t) = k^2 D(k,t)$ and

$$\lim_{k\to 0} D(k,t) = \langle v_z(0)v_z(t)\rangle.$$

Since

$$D = \int_0^\infty \mathrm{d}t \langle v_z(0)v_z(t)\rangle$$

we obtain that $\hat{D}(k\to 0, z=0) = D$ and

$$\lim_{k\to 0} F_s(k,t) = \exp(-Dk^2|t|). \tag{48}$$

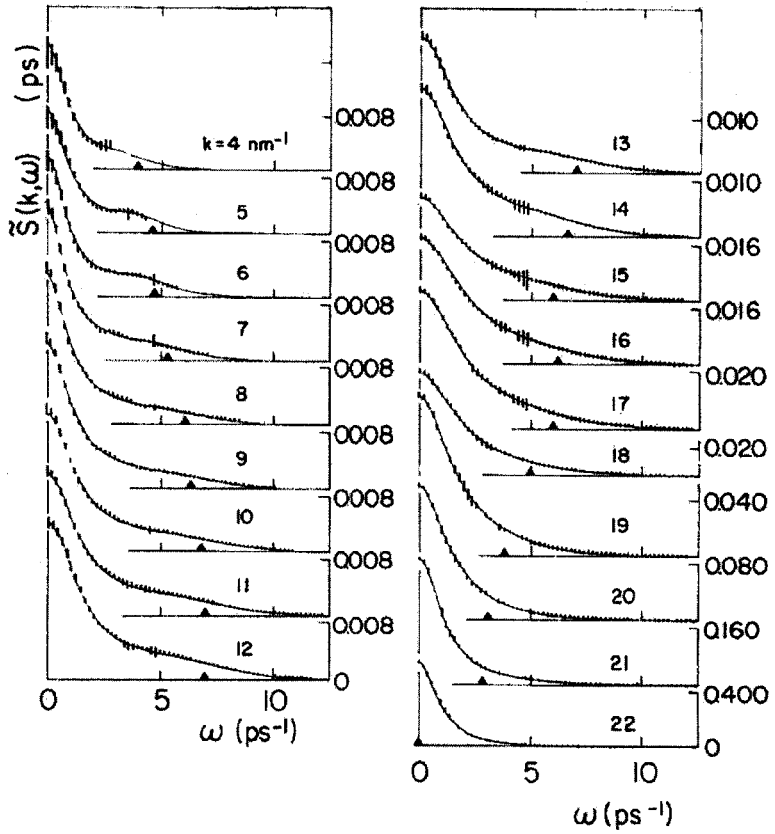

Figure 1. Dynamic structure factor of dense Ne (density 34.62 nm^{-3}). Error bars: experimental data. Solid line: fit with the three Lorentzian model. The triangles show the frequencies of the propagating mode.

2.5.2. Mode coupling. The memory function formalism is based on the assumption that the random force $\vec{K}(t)$ is orthogonal to the set of slowly varying variables. This does not mean that $\vec{K}$ is orthogonal to combinations of the form AA or AAA etc. Since these combinations will have slowly varying features, not all slow parts of $\vec{K}$ are projected out. In order to improve our approximations for the memory function M we may define a new projection operator that projects any variable onto the subspace spanned by AA. Applying the procedure to single-particle motion we may choose not only $\rho^1_{\vec{k}}$, but also the current $\vec{j}_{\vec{k}}$. This choice is based on MD simulations by Alder and Wainwright (1970), who observed that a moving particle in a liquid creates a vortex or backflow in the bath of surrounding particles, which in turn leads to a slow-down of the decay of the velocity autocorrelation function. The result is

$$Z(t) = \frac{1}{3\rho(2\pi)^3}\int \mathrm{d}\vec{k}\frac{F_s(k,t)}{k^2}[C_L(k,t) + 2C_T(k,t)] \tag{49}$$

which in the hydrodynamic limit turns into

$$Z(t) = \frac{2k_BT}{3\rho M(2\pi)^3}\int \mathrm{d}\vec{k}\exp[-(D+\nu)k^2t]. \tag{50}$$

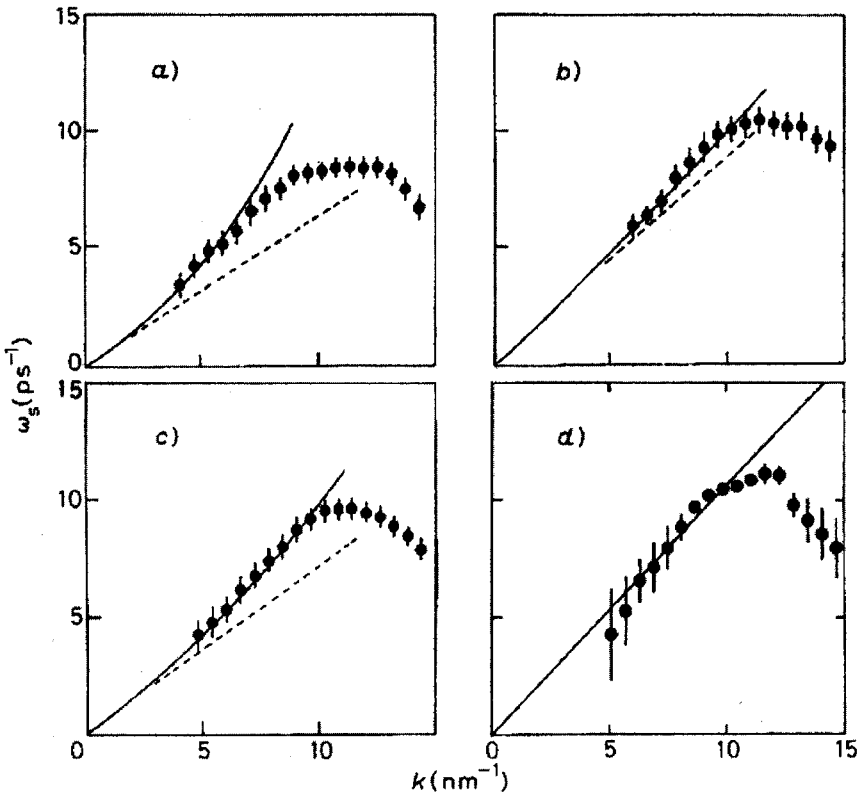

Figure 2. Sound dispersion in liquid argon determined from neutron scattering (dots with error bars), linearized hydrodynamics (dashed lines) and mode-coupling theory (solid lines) at four densities (in nm^{-3}): (a) 17.60, (b) 18.51, (c) 20.11, (d) 21.63.

For $t \to \infty$ (which is appropriate in the hydrodynamic limit) this can be written as

$$Z(t) \approx \frac{2k_BT}{3\rho M}[4\pi(D+\nu)t]^{-3/2}. \tag{51}$$

The Fourier transform of $Z(t)$ for small frequencies is then (de Schepper and Ernst 1979):

$$\tilde{Z}(\omega) \approx D - \frac{\sqrt{2}k_BT}{12\pi M\rho(D+\nu)^{3/2}}\sqrt{\omega}. \tag{52}$$

Mode-coupling results are also reflected in the small k behaviour of the self-intermediate scattering function, and correspondingly in $S_s(k,\omega)$, as well as in the dispersion relation, which shows the positions of the peaks of $C_L(k,\omega)$ as a function of k. For instance (de Schepper and Ernst 1979):

$$F_s(k,t) = \exp(-Dk^2t) - \frac{k}{k^*}\exp(-\tau+\tau\delta)W(\tau\delta) \tag{53}$$

with $\tau = Dk^2t$, $k^* = 4\pi M\rho D(D+\nu)/(k_BT)$, $\delta = D/(D+\nu)$ and

$$W(x) = \frac{1}{4\sqrt{\pi}}\frac{1}{\sqrt{x}}\left[\frac{1}{\sqrt{x}}\mathcal{F}(\sqrt{x})(4x^2-4x+1) - 2x + 1\right]$$

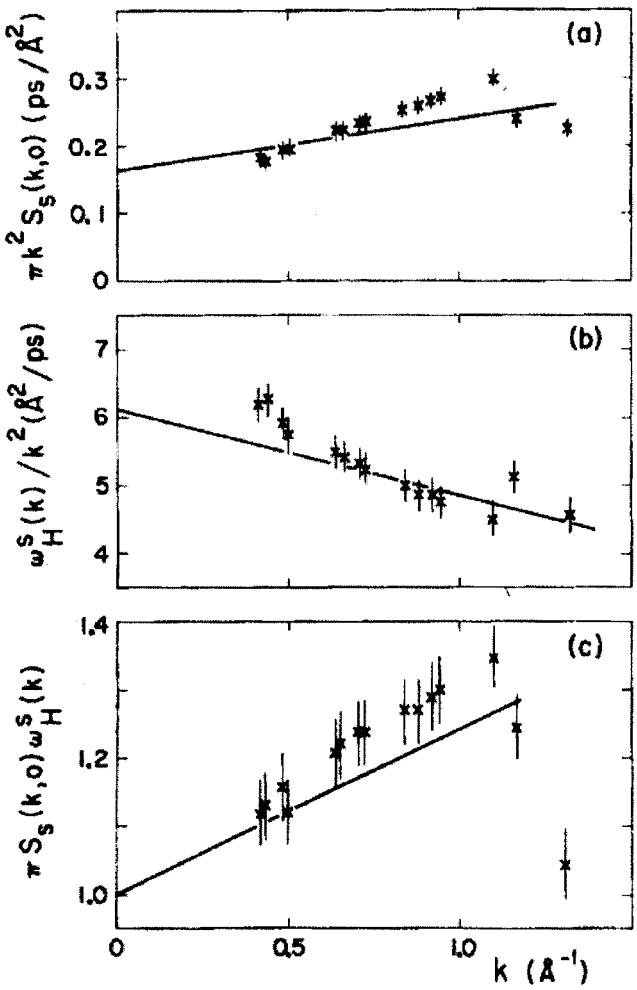

Figure 3. Comparison of experimental data for the self-dynamic structure factor of dense hydrogen gas (density 21.2 nm^{-3}) with the predictions of mode-coupling theory. (a) Initial value. (b) Half width at half maximum, and (c) their product. The crosses with error bars denote the experimental data. The lines are the mode-coupling predictions.

with $\mathcal{F}(y) = \sqrt{\pi}\,\mathrm{i}\exp(-y^2)\,\mathrm{erf}(-\mathrm{i}y)/2$. This leads to a value of $S_s(k, \omega = 0)$ and a half-width at half maximum $\omega_H^s(k)$ which behave as

$$k^2 S_s(k, 0) = \frac{1}{D\pi}(1 + \alpha k) \qquad \frac{\omega_H^s(k)}{k^2} = D(1 - \beta k). \tag{54}$$

Moreover, the behaviour of the function $Z(k, \omega)$ for small k is given by

$$Z(k, \omega) = \tilde{Z}(\omega) + \mathrm{O}(k^2)$$

i.e. linear terms in k are absent. Also we have, for the dispersion relation,

$$\omega_s(k) = c_s k + \mu k^{5/2} \tag{55}$$

where the values of α, β and μ are given basically in terms of transport coefficients and thermodynamic properties. It is observed that in all cases these mode-coupling effects appear as corrections, for small k, of the corresponding hydrodynamic expressions.

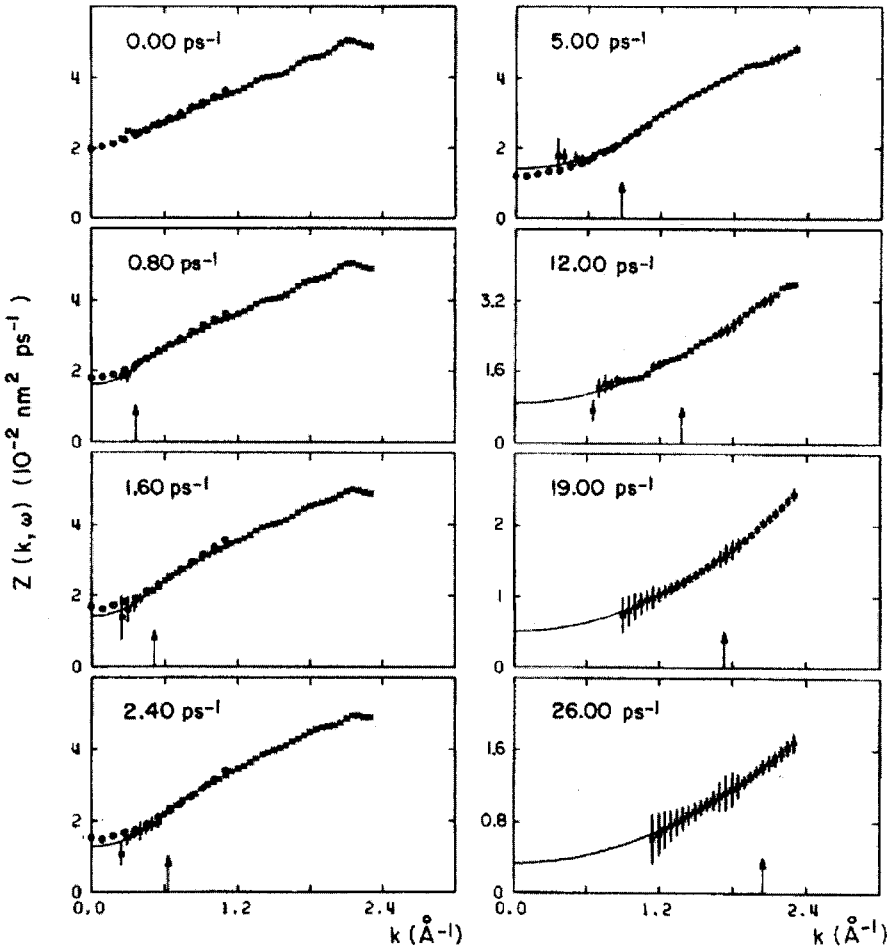

Figure 4. The function $Z(k, \omega)$ of dense hydrogen gas for several values of the frequency. For each frequency a quadratic extrapolation to $k = 0$ is shown, although a linear extrapolation could also be tried (see the next figure). The value obtained for $k = 0$ is the Fourier transform of the velocity autocorrelation function.

3. Experimental results and computer simulations

Inelastic neutron scattering and high-resolution inelastic x-ray scattering are the two probes to investigate the microscopic dynamics in condensed matter. X-rays are scattered by the electrons of the atoms and the scattered intensity is proportional to $Z^2 r_e^2$, with Z the atomic number and $r_e = 2.818$ fm the classical electron radius. For example, for H we have $Z^2 r_e^2 = 7.9$ fm^2 and for Pb it is 53 400 fm^2. In contrast (except in the case of magnetic scattering) neutrons are scattered by the atomic nuclei with an intensity proportional to $\langle b^2 \rangle$ with b the scattering length. For example, for H and Pb we have $\langle b^2 \rangle = 653$ and 88 fm^2 respectively. The neutron has spin $1/2$ and as a consequence if the nucleus has a spin the neutron–nucleus interaction depends on the orientation of the neutron spin with respect to the nuclear spin. For example, when a neutron is scattered by a proton we have $b_+ = +10.9$ fm for parallel spins and $b_- = -47.5$ fm for anti-parallel spins. If the nuclei of a monatomic system have randomly distributed spin

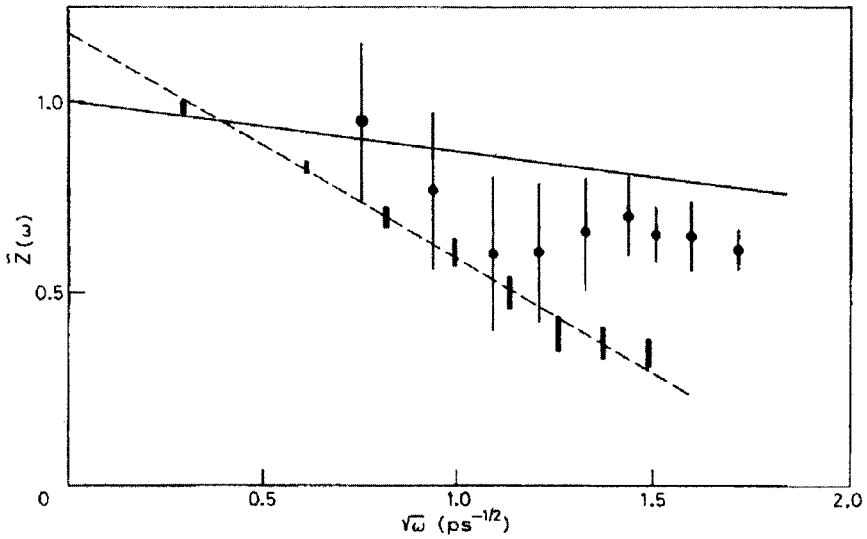

Figure 5. Fourier transform of the velocity autocorrelation function for dense hydrogen gas compared with mode-coupling predictions (full line). Dots with error bars are the results from the quadratic extrapolation shown in the previous figure. Error bars without symbols denote the results of a linear extrapolation of the same data. Note that they also fit to a straight line (dashed line), which is the mode-coupling behaviour, but the slope is too large compared to the mode-coupling result.

orientations, the scattered intensity will in general have a coherent and an incoherent component proportional respectively to $\langle b\rangle^2$ and to $\langle b^2\rangle - \langle b\rangle^2$; for H respectively 14 and 639 fm. Different isotopes of one element generally have different scattering lengths, which also leads to coherent and incoherent scattering in the case of spatial random distribution.

Coherent scattering is proportional to $S(k, \omega)$, while incoherent scattering is proportional to $S_s(k, \omega)$. This is a complication in the case of neutrons unless one of the two components is dominant, as in the case of a single isotope without nuclear spin (e.g. ^{36}Ar, a purely coherent scatterer) or e.g. in the case of H (mainly incoherent scattering). The latter case demonstrates one of the advantages of neutrons, because it is impossible to measure $S_s(k, \omega)$ with x-rays.

Various methods are available to measure $S(k, \omega)$ as well as $S_s(k, \omega)$ of one element: (a) using polarized neutron beams and the fact that the neutron spin flips in incoherent scattering, (b) neutron scattering using two samples of different isotopic composition or (c) combining neutrons and x-rays.

3.1. Simple fluids

The first experimental observation of collective modes propagating in a fluid with wavelength comparable to the interparticle distance was in a neutron scattering experiment on liquid Rb (mainly coherent) by Copley and Rowe (1974). They observed clear inelastic peaks in $S(k, \omega)$ for $3 < k < 10$ nm^{-1}. The dispersion curve for the position appeared as a continuation of the sound dispersion. The results agreed very well with MD simulations by Rahman (1974a, b).

Inspired by this result, de Schepper *et al* (1983) fitted equation (40) with $j = -1, 0, +1$, i.e. the expression for extended hydrodynamics, to neutron scattering data at $4 < k < 38$ nm^{-1} for liquid ^{36}Ar. Although no inelastic peaks were visible, the experimental data could be very well described even up to $k = 38$ nm^{-1} by the extended hydrodynamic modes. Similar results

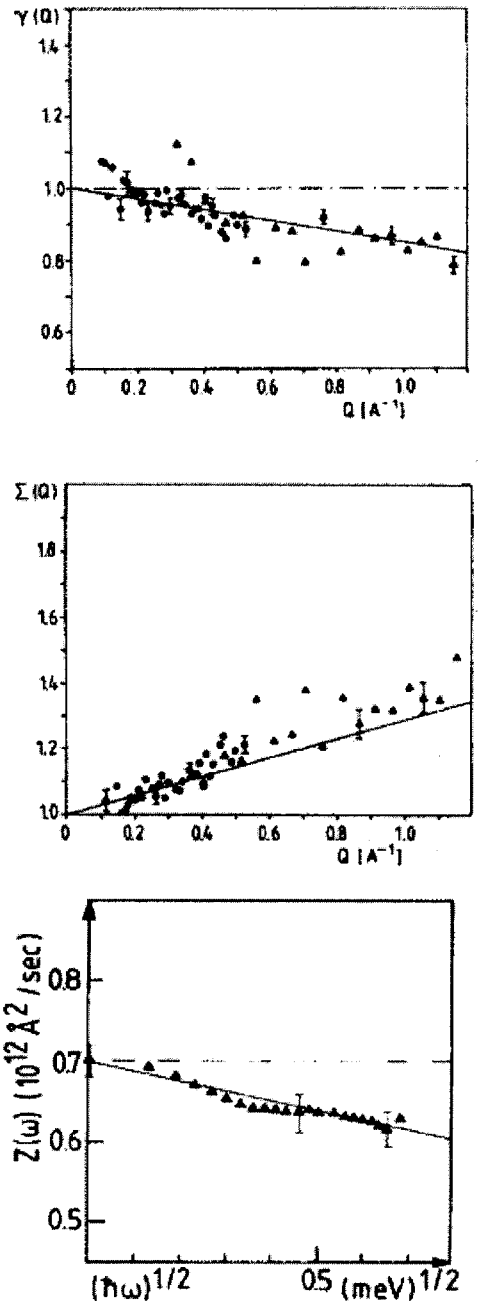

Figure 6. Comparison of experimental data for liquid Na with mode-coupling behaviour. Top panel: normalized half width at half maximum of $S_s(k, \omega)$. Central panel: normalized initial value of $S_s(k, \omega)$. Bottom panel: Fourier transform of the velocity autocorrelation function, obtained through linear extrapolation to $k = 0$ of $Z(k, \omega)$ data.

were found for liquid Ne (mainly coherent) by van Well and de Graaf (1985) (figure 1). At the lower limit of the k-range it was not possible to verify that the extended modes are indeed a continuation of the real hydrodynamic modes. However, within the experimental range of k,

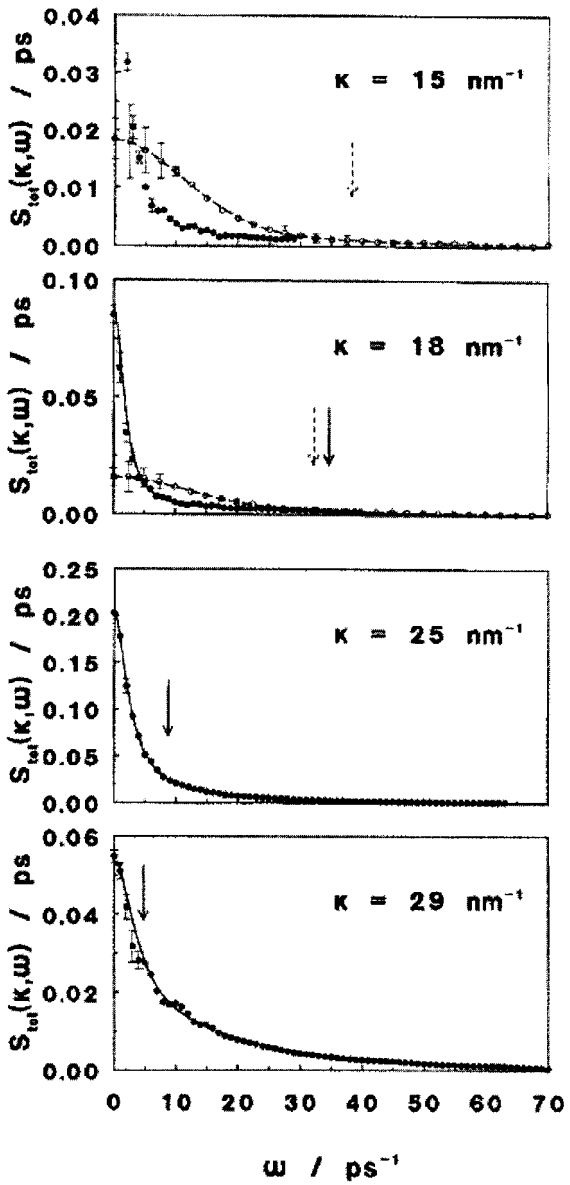

Figure 7. Total dynamic structure factor (weighted sum of $S(k, \omega)$ and $S_s(k, \omega)$ according to the corresponding coherent and incoherent cross sections) measured for different incident neutron energies: full circles, $E_0 = 20.5$ meV; open circles, $E_0 = 524.8$ meV. Note that the resolution function is much broader for the higher incident energy (see the next figure). Lines are fits to the data using a three Lorentzian model for $S(k, \omega)$ and the arrows show the frequencies of the propagating modes for each set of data.

the presence of mode-coupling effects could be demonstrated unambiguously, not only in the dispersion relation of liquid argon (figure 2), but also in $S_s(k, \omega)$ for high-density hydrogen gas (Verkerk *et al* 1985) (figure 3) and for the velocity autocorrelation function in hydrogen (Verkerk 1990) (figures 4 and 5) as well as liquid Na (Morkel *et al* 1987) (figure 6).

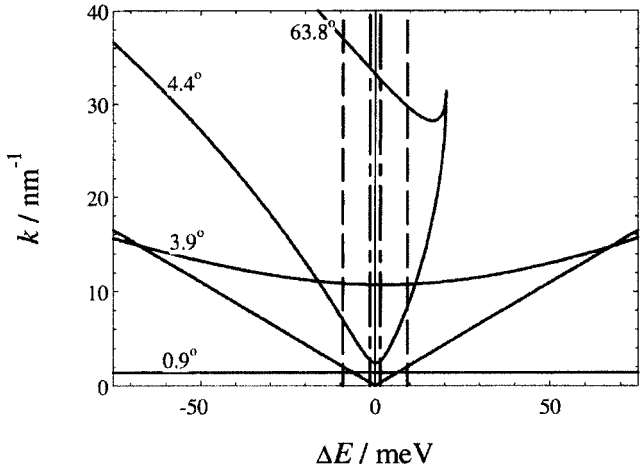

Figure 8. Kinematically allowed $(k, \Delta E)$ region for neutrons of different incident energies. The lines for 4.4 and 63.8 degrees (scattering angle) are for neutrons with $E_0 = 20.5$ meV. The dash–dotted vertical line is the half width at half maximum (HWHM) of the resolution function. The slanted straight lines show the expected position of the side peaks in $S(k, \omega)$ for liquid Li as obtained from the hydrodynamic speed of sound, which clearly falls outside the allowed range for these k values. The lines for 0.9 and 3.9 degrees correspond to incident energy 524.8 meV, whereas the dashed vertical lines show the HWHM of the corresponding resolution function.

In the investigation of liquid Li (figure 7) with its high sound velocity (4500 m s^{-1}), the kinematic limitations of inelastic neutron scattering became very apparent (de Jong *et al* 1993). This is due to the relation for conservation of momentum and energy of the neutron in a scattering experiment:

$$k^2 = k_0^2 + k_1^2 - 2k_0k_1\cos\varphi$$
$$\Delta E = \hbar^2(k_1^2 - k_0^2)/(2m) \tag{56}$$

leading to

$$k^{*2} = 2 - \Delta E^* - 2\sqrt{1 - \Delta E^*}\cos\varphi \tag{57}$$

with $\hbar k$ the momentum transfer, k_0 and k_1 the wavevectors of the incident and scattered neutron, $k^* = k/k_0$, φ the scattering angle, $\Delta E = \hbar\omega$ the energy transfer, $\Delta E^* = \Delta E/E_0$, with E_0 being the energy of the incident neutron, and m the neutron mass. Obviously, only a restricted area of (k, ω) space is accessible in a neutron scattering experiment, where φ is constant. Note also that for the energy loss side, there is a maximum value of ΔE when the neutron loses all of its incident energy. In the case of photons, the energy transfer is given by $\hbar\omega = \Delta E = \hbar c(k_1 - k_0)$, with c the speed of light. Because c is very large and for x-ray scattering ΔE is very small (of the order of meV) as compared to the incident photon energy (of the order of keV), $k_1 \approx k_0$ to a very good approximation and consequently for inelastic x-ray scattering we take $k = 2k_0\sin(\varphi/2)$, which is now independent of ΔE (figure 8).

In 1987 the technique of inelastic x-ray scattering was sufficiently advanced (Dorner, Burkel, Peisl, Sinn; see Burkel 1991, and references therein) to perform the first experiments on liquid Li investigating propagating modes. The resolution was 26 meV, i.e. 2×10^{-6} of the incident energy. Today, this technique is further refined and a resolution of 1.5 meV is possible. Liquid lithium (Scopigno *et al* 2000) has been recently remeasured and the results are shown in figure 9.

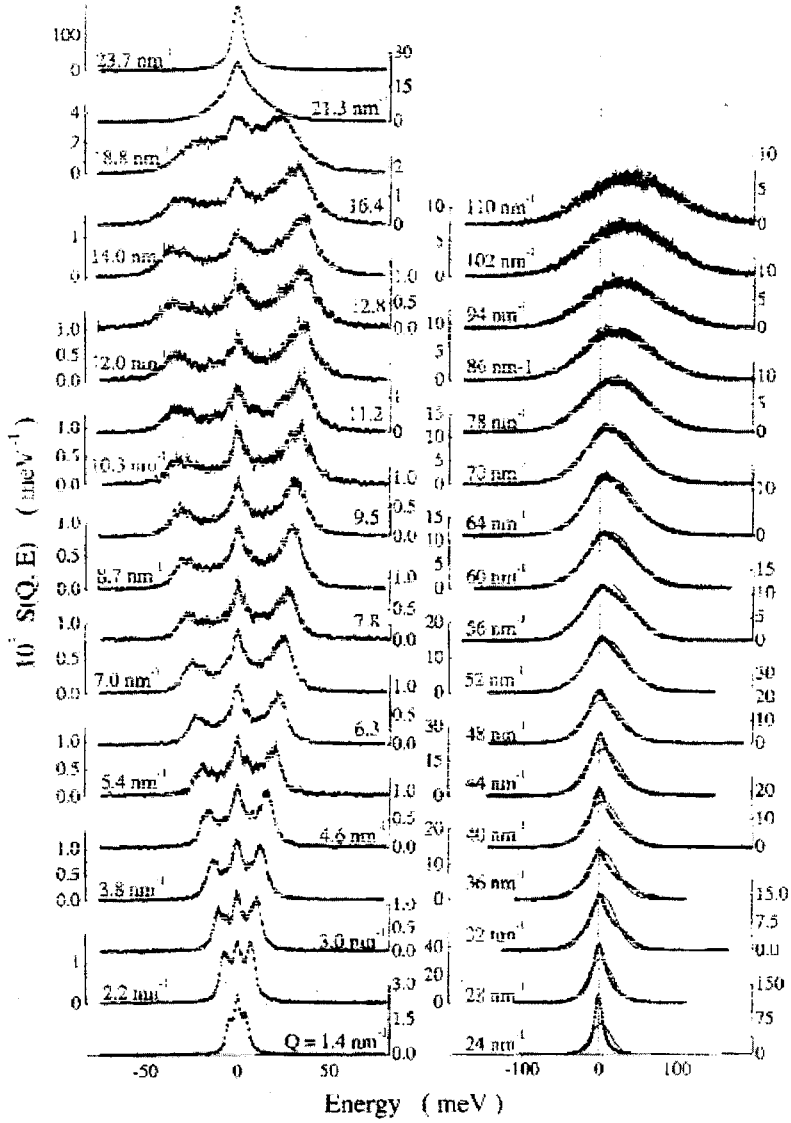

Figure 9. Dynamic structure factor of liquid Li near melting, measured by inelastic x-ray scattering, for several wavevectors. The full line in the right panel is the expected free particle limit.

Neutron scattering experiments were performed at lower k by combining high energy resolution with small-angle scattering, sometimes called neutron Brillouin scattering, because in the low-k, hydrodynamic limit, $S(k, \omega)$ should approach the Rayleigh–Brillouin triplet, equation (34). The first data using this technique were obtained at room temperature for dense N_2 gas (mainly coherent) (27 and 51 MPa) by Egelstaff *et al* (1989) and for dense ^{36}Ar gas (8 and 20 MPa) by Bafile *et al* (1990), see figure 10. In both cases extended hydrodynamic modes were observed which were a smooth continuation of the hydrodynamic modes, with the transition somewhere between $k = 0.5$ and 1.0 nm^{-1}. More recently, the experimentally more difficult case of liquid ^{36}Ar was investigated also with neutron Brillouin scattering by Mos *et al* (1997). For $k = 0.85$ nm^{-1} the results agreed well with the hydrodynamic model.

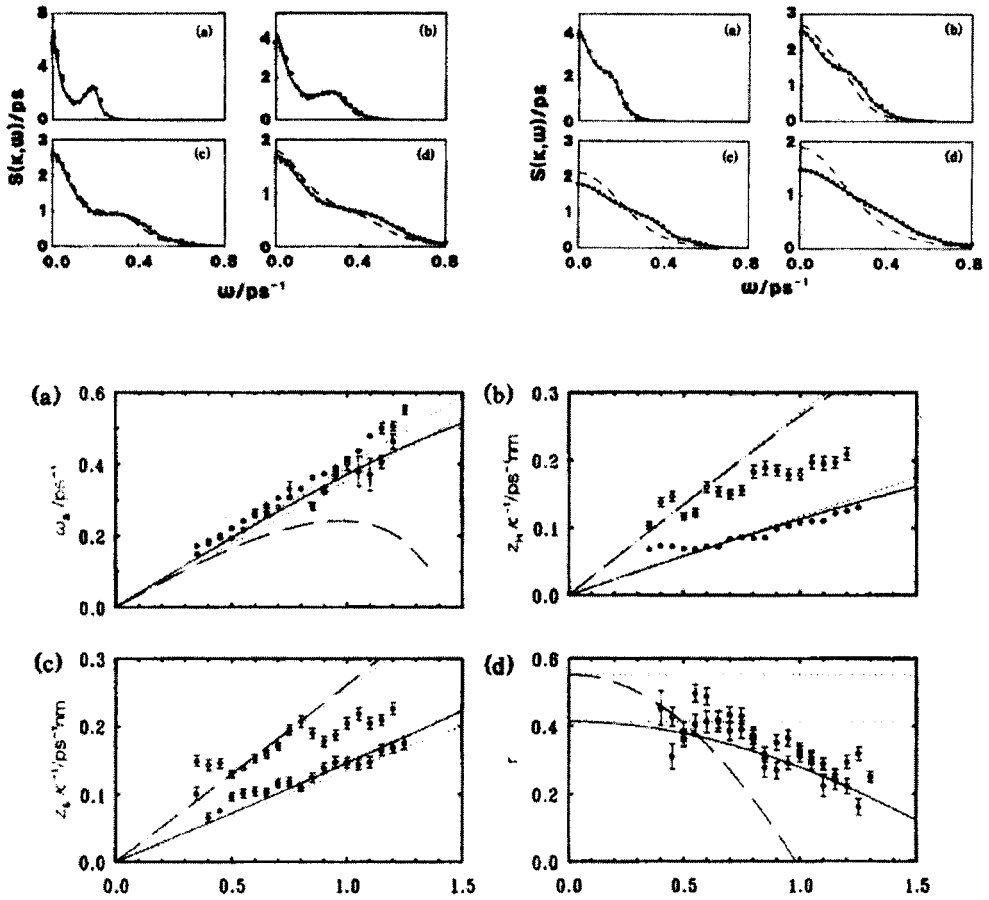

Figure 10. Results of neutron Brillouin scattering on dense Ar. Upper panel, left: results for density 5.04 nm^{-3}. Dots: experiment. Broken line: linearized hydrodynamics. Full line: fit with a three Lorentzian model. (a) $k = 0.5\ nm^{-1}$, (b) $k = 0.75\ nm^{-1}$, (c) $k = 1.00\ nm^{-1}$, (d) $k = 1.25\ nm^{-1}$. Upper panel, right: results for density 2.00 nm^{-3}. Symbols and k values are as in the left panel. Lower panels: variation of the parameters in the fit with the three Lorentzian model with k for both densities: full symbols, higher density; open symbols, lower density. Lines show the hydrodynamics predictions: full line, higher density; dashed line, lower density. (a) Position of the sound mode, (b) width of the heat mode, (c) width of the sound mode, (d) ratio between the amplitudes of the sound mode and the heat mode.

The combination of neutron Brillouin scattering and the strongly and coherently scattering isotope ^{36}Ar made it possible to investigate the dynamics at low density and in the region where in a hard-sphere system binary uncorrelated collisions would be dominant over higher order collisions (Verkerk *et al* 1991) (figure 11). This means that if equation (41) is rewritten as $S(k,\omega) = S^{(0)}(k,\omega) + \rho S^{(1)}(k,\omega) + \mathrm{O}(\rho^2)$, then the higher order terms should be negligible. The experiment showed that $S^{(1)}(k,\omega)$ for ^{36}Ar is quite different from the hard-sphere one, which is given in terms of the density-independent and k-independent function $s^B_{11}(\omega^*)$ and also from the function corresponding to a Lennard-Jones fluid (Barocchi *et al* 1996) although the differences with this case diminish as k decreases. Therefore this function is a quite sensitive test of the interatomic potential.

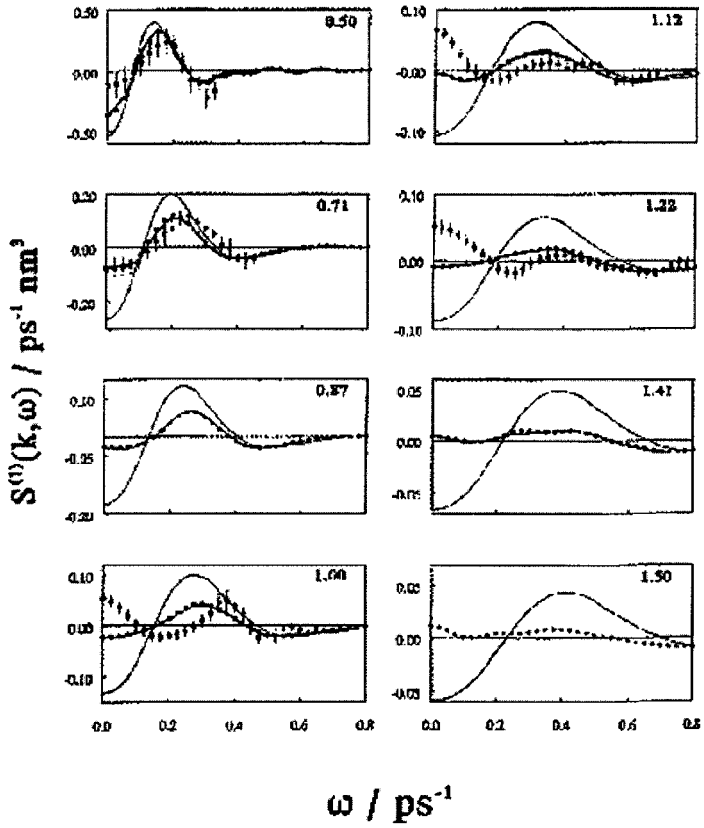

Figure 11. First order correction of the free particle dynamic structure factor measured for dense Ar compared with results for several interatomic potentials. Dots: experimental data. Symbols with error bars: results for a Lennard-Jones fluid. Line: results for hard spheres.

3.2. Binary mixtures

The MD simulation of liquid Li_4Pb by Jacucci *et al* (1984) lead to a strong increase of interest in liquid binary mixtures with disparate masses, in particular in the phenomenon of fast sound. The first experimental indications for the existence of fast sound came from neutron experiments on liquid He–Ne by Montfrooij *et al* (1989). The results are confirmed by combined neutron scattering and MD simulation of He–Ar by Crevecoeur *et al* (1996). MD simulations of liquid He–Ne by Enciso (1995) showed that the fast and the slow mode both converge to the hydrodynamic mode with decreasing k. This picture differs from the kinetic model calculations of Westerhuijs *et al* (1992).

The same problem as with inelastic neutron scattering on liquid Li turned up in experiments on liquid Li_4Pb (de Jong *et al* 1994, Alvarez *et al* 1998). However, because of the extremely large scattering cross section of Pb for x-rays, inelastic x-ray experiments would be extremely hard or even impossible. In both neutron experiments the existence of a high-frequency mode was confirmed (figures 12 and 13). New MD simulations of liquid Li_4Pb by Fernandez-Perea *et al* (1998) (figure 14) support the conclusions from the more recent neutron scattering experiment that the high-frequency mode is supported by the Li atoms only, but that the character is rather different from the sound mode in pure Li: it is more or less localized

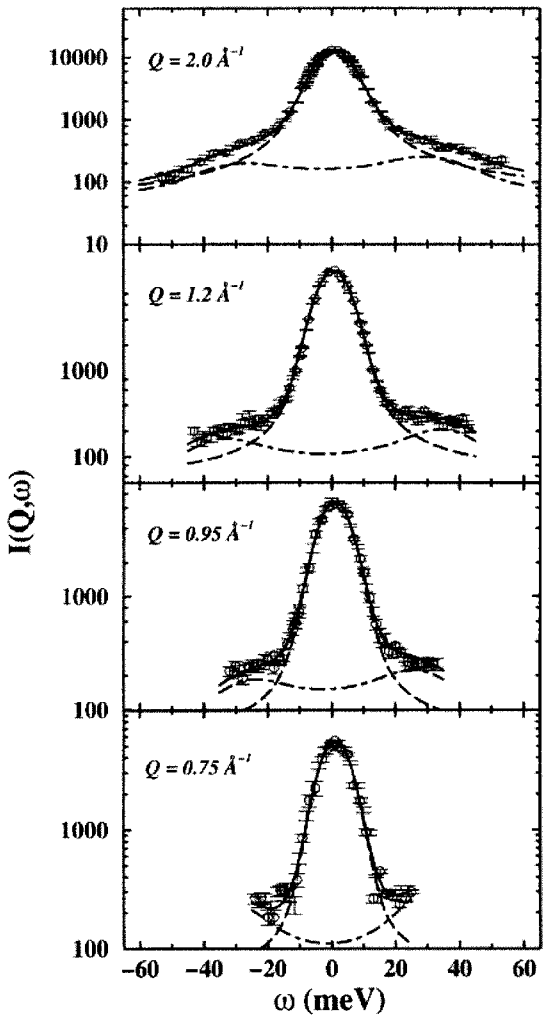

Figure 12. Inelastic neutron scattering spectra of liquid Li_4Pb at several wavevectors. Symbols are experimental data, and lines are fits to the full data (solid line) and the corresponding quasielastic (dashed line) and inelastic (dash–dotted line) components.

and shows features of optical modes. Recently, the existence of optical transverse modes in liquid Li_4Pb has been predicted by Bryk and Mryglod (2000), while in a He–Ar mixture the high-frequency modes are kinetic, which means they disappear in the hydrodynamic limit (Crevecoeur *et al* 1996).

4. Summary

Our knowledge of fundamental dynamical properties of liquids has considerably increased over the last decades thanks to the close collaboration of theory, computer simulation and neutron scattering and in the last decade also inelastic x-ray scattering. This is of great importance for understanding macroscopic phenomena in simple and complicated liquids and for the improvement of technological processes.

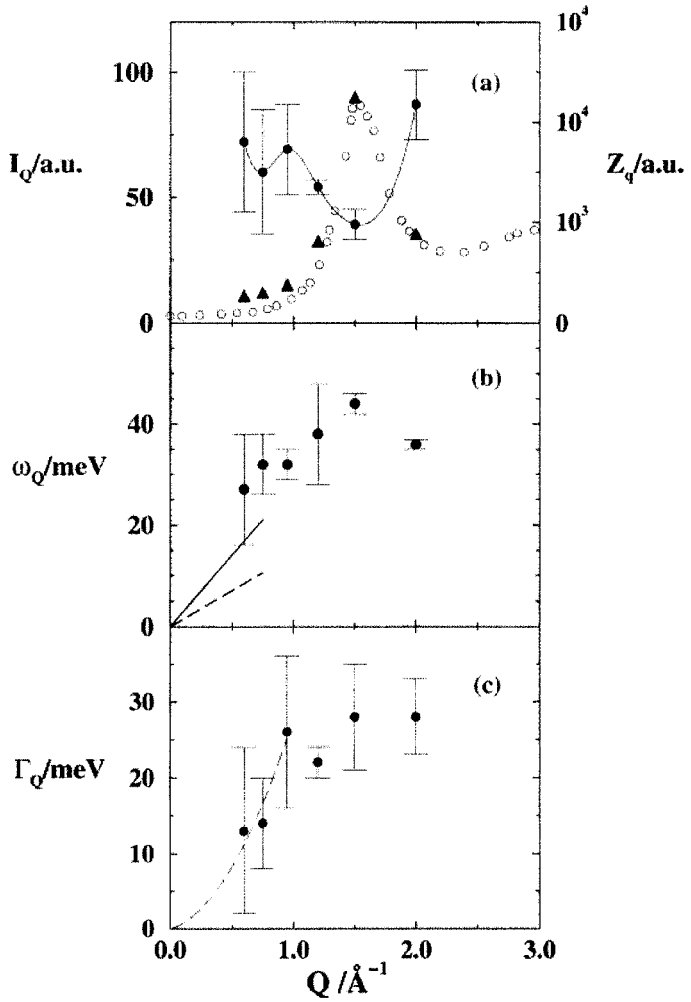

Figure 13. The upper panel (a) shows the Q dependence of the integrated intensities of the quasielastic Z_q (triangles) and inelastic I_q (full circles) components of the spectra, while open circles denote the static structure factor, scaled to Z_q. The central panel (b) shows the positions of the inelastic peaks (circles with error bars) together with the expected positions for hydrodynamic sound of Li_4Pb (dashed line) and pure Li (solid line). The lower panel (c) shows the full width of the inelastic peaks, while the dashed line is an estimate of the hydrodynamic damping law.

Theoretical approaches summarized in this paper are short-time expansion, the free gas model, the visco-elastic model, the damped harmonic oscillator, (generalized) hydrodynamics, the Boltzmann theory for low density, the Enskog theory for hard spheres and mode coupling theory.

The development of high-resolution inelastic x-ray scattering opens new possibilities, in particular in combination with neutron scattering.

4.1. Challenges

Neutron Brillouin scattering and inelastic x-ray scattering may help us to understand more about the transition from the microscopic (kinetic) regime to macroscopic hydrodynamics. Neutron

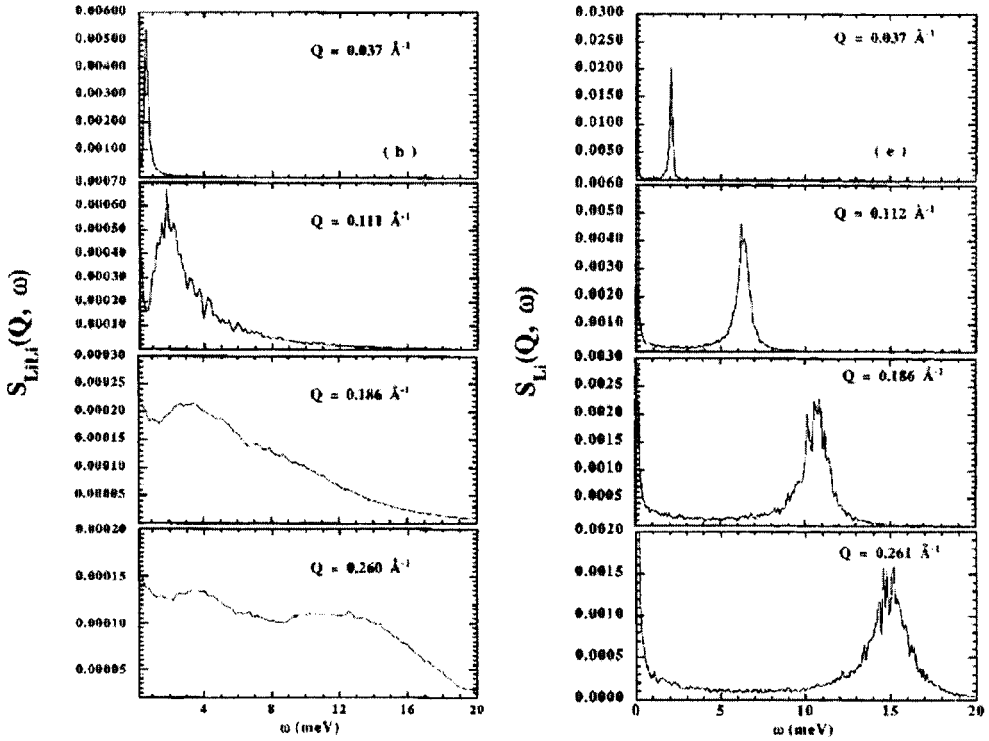

Figure 14. Left panels: calculated Li–Li partial dynamic structure factor in the Li_4Pb liquid alloy. Right panel: calculated dynamic structure factor of pure liquid Li.

Brillouin scattering is the unique tool to further investigate deviations from the regime where binary collisions are dominant. It might turn out to be imperative to combine neutrons and x-rays for investigating processes like nucleation and chemical reactions, or complex systems, even biological systems. Other challenges are liquids under extreme conditions, for instance to understand the physics of the interior of the earth and other planets (the interior of Jupiter and Saturn contains metallic fluid hydrogen).

To date the number of new applications of the intense radiation available at the latest generation of electron synchrotrons seems to expand continuously. It is believed that the advent of future neutron sources like SNS in the USA or the European Spallation Source will lead to a similar situation for neutrons. In any case it will be necessary to use the synergy of x-rays combined with neutrons to meet challenges like the ones mentioned above.

References

Ailawadi N K, Rahman A and Zwanzig R 1971 *Phys. Rev.* A **4** 1616
Alder B J and Wainwright I E 1970 *Phys. Rev.* A **1** 18
Alvarez M, Bermejo F J, Verkerk P and Rössli B 1998 *Phys. Rev. Lett.* **80** 2141
Barocchi F, Bafile U and Magli R 1996 *J. Phys.: Condens. Matter* **8** 9111
Bafile U, Verkerk P, Barocchi F, de Graaf L A, Suck J-B and Mutka H 1990 *Phys. Rev. Lett.* **65** 2394
Bryk T and Mryglod I 2000 *J. Phys.: Condens. Matter* **12** 6063
Burkel E 1991 *Inelastic Scattering of X-Rays with Very High Energy Resolution* (Berlin: Springer)
Chapman S and Cowling T G 1970 *The Mathematical Theory of Non-Uniform Gases* 3rd edn (Cambridge: Cambridge University Press)

Cohen E G D and de Schepper I M 1990 *Nuovo Cimento* D **12** 521
Copley J R D and Rowe J M 1974 *Phys. Rev. Lett.* **32** 49
Crevecoeur R M, Smorenburg H E and de Schepper I M 1996 *J. Low Temp. Phys.* **105** 149
Cunsolo A, Pratesi G, Ruocco G, Sampoli M, Sette F, Verbeni R, Barocchi F, Krisch M, Masciovecchio C and Nardone M 1998 *Phys. Rev. Lett.* **80** 3515
de Jong P H K, Verkerk P and de Graaf L A 1993 *J. Non-Cryst. Solids* **156–158** 48
de Jong P H K, Verkerk P, de Vroege C F, de Graaf L A, Howells W S and Bennington S M 1994 *J. Phys.: Condens. Matter* **6** L681
de Schepper I M and Ernst M H 1979 *Physica* A **98** 189
de Schepper I M, Verkerk P, van Well A A and de Graaf L A 1983 *Phys. Rev. Lett.* **50** 974
DeGennes R G 1959 *Physica* **25** 825
Egelstaff P A, Kearley G, Suck J-B and Youden J P A 1989 *Europhys. Lett.* **10** 37
Fernandez-Perea R, Alvarez M, Bermejo F J, Verkerk P, Rössli B and Enciso E 1998 *Phys. Rev.* E **58** 4568
Frenkel J 1946 *Kinetic Theory of Liquids* (Oxford: Clarendon) p 196
Hansen J-P and McDonald I R 1986 *Theory of Simple Liquids* (London: Academic)
Jacucci G, Ronchetti M and Schirmacher W 1984 *J. Physique Coll.* **8** C8 385
Kamgar-Parsi B, Cohen E G D and de Schepper I M 1987 *Phys. Rev.* A **35** 4781
Levesque D, Verlet L and Kürkijarvi J 1973 *Phys. Rev.* A **7** 1690
Maitland G C, Rigby M, Smith E B and Wakeham W A 1981 *Intermolecular Forces* (Oxford: Clarendon)
Maxwell J C 1867 *Phil. Trans.* **157** 49
Montfrooij W, Westerhuijs P, de Haan V O and de Schepper I M 1989 *Phys. Rev. Lett.* **63** 544
Morkel C, Gronemeyer C and Gläser W 1987 *Phys. Rev. Lett.* **58** 1873
Mos B, Verkerk P, Bafile U, Benmore C, Suck J-B, Barocchi F, Cook J and Andersen K 1997 *Physica* B **234–236** 308
Puff R D 1965 *Phys. Rev.* **137** 406
Rahman A 1974a *Phys. Rev. Lett.* **32** 52
——1974b *Phys. Rev.* A **9** 1667
Scopigno T, Balucani U, Cunsolo A, Masciovecchio C, Ruocco G, Sette F and Verbeni R 2000 *Europhys. Lett.* **50** 189
van Beijeren H and Ernst M H 1973 *Physica* **68** 437
——1979 *J. Stat. Phys.* **21** 125
van Well A A and de Graaf L A 1985 *Phys. Rev.* A **32** 2396
Verkerk P 1990 *Nuovo Cimento* D **12** 441
Verkerk P, Bafile U, Barocchi F, de Graaf L A, Suck J B and Mutka H 1991 *Phys. Rev. Lett.* **67** 1262
Verkerk P, Builtjes J H and de Schepper I M 1985 *Phys. Rev.* A **31** 1731
Westerhuijs P, Montfrooij W, de Graaf L A and de Schepper I M 1992 *Phys. Rev.* A **45** 3749